Optical bands and energy levels of Nd^{3+} ion in the $YAl_3(BO_3)_4$ nonlinear laser crystal

1997 J. Phys.: Condens. Matter 9 9715

(http://iopscience.iop.org/0953-8984/9/44/024)

J. Phys.: Condens. Matter **9** (1997) 9715–9729. Printed in the UK PII: S0953-8984(97)83668-5

Optical bands and energy levels of Nd^{3+} ion in the $YAl_3(BO_3)_4$ nonlinear laser crystal

D Jaque†, J Capmany†, Z D Luo‡ and J García Solé†

† Departamento de Física de Materiales, Universidad Autónoma de Madrid, Cantoblanco, 28049 Madrid, Spain

‡ Fujian Institute of Research on The Structure of Matter, Chinese Academy of Sciences, Fuzhou, Fujian 350002, People's Republic of China

Received 24 April 1997, in final form 13 August 1997

Abstract. In this paper the polarized optical spectra (absorption and fluorescence) of the Nd^{3+} ion in the $YAl_3(BO_3)_4$ nonlinear crystal have been systematically investigated at low (10 K) and room temperature. Most energy levels of Nd^{3+} in this crystal (103) have been identified and conveniently labelled with their crystal field quantum numbers, $\mu = 1/2$ and $\mu = 3/2$. The radiative emitting states have been identified. Analysing the optical absorption spectra with the anisotropic Judd–Ofelt theory, the radiative lifetimes and branching ratios from the metastable state $^4F_{3/2}$ have been calculated. Then, relevant spectroscopic parameters (quantum efficiency and emission cross sections) for laser applications have been estimated. Infrared to visible up-conversion is reported for the first time in this host crystal.

1. Introduction

The increasing interest in small compact diode-pumped lasers in the blue–green spectral domain has supported the research on new solid state laser systems based on nonlinear crystals [1, 2]. These crystals, when activated with trivalent rare earth ions, provide the possibility of realizing diode-pumped visible lasers by self-frequency-doubling (SFD) the main infrared laser radiation lines.

Yttrium aluminum borate, $YAl_3(BO_3)_4$ (hereafter referred to as YAB), is a nonlinear crystal which has proved to be an excellent host for Nd^{3+} ions in order to produce green laser radiation at 530 nm by SFD its infrared laser line at 1.06 μm. In fact, this laser system has been operated under a variety of schemes [3–7] and continuous-wave (cw) green powers up to 50 mW have been reached [6]. Thus, it appears to be an excellent system in relation to the other two existing SFD cw lasers, $LiNbO_3$:MgO:Nd [8] and $LaBGeO_5$:Nd [9–12].

In spite of the fact that some papers [13–15] have partially dealt with the optical properties of Nd^{3+} in YAB, a full characterization of the spectroscopy of this material is still lacking. This characterization is necessary in order to attain a full understanding of the laser gain properties of this ion–host combination, so that its performance can be predicted.

This paper presents a systematic investigation of the optical (absorption and luminescence) bands of Nd^{3+} in YAB. By a careful investigation of the location of these bands a complete table of the energy levels of Nd^{3+} ion, conveniently labelled, is provided. This table together with the analysis of the band intensities and fluorescence lifetimes is used to estimate some relevant laser parameters of the main emission in the laser channel.

0953-8984/97/449715+15$19.50

In addition, infrared to visible up-converted fluorescence is reported for the first time in this material.

2. Crystal properties and experimental details

Single crystals of Nd:YAB were grown by the flux method with a modified molybdate flux system at the Institute of Structure of Matter (Fuzhou, China). The mixture of starting materials was fired at a temperature about 1100 °C, kept for twelve hours and then cooled down to the saturation temperature which was measured by repeating seeding. A seed was transferred down into the melt and rotated at a rate of 9–30 rpm and the temperature of the melt was cooled down at a rate of 1.5–2 °C d^{-1} to about 900 °C.

The yttrium aluminum borate crystal belongs to the space group $R32$ of the trigonal system, having lattice parameters $a = 0.9293$ nm, $b = 0.9293$ nm and $c = 0.7245$ nm [16]. Nd^{3+} ions enter Y^{3+} sites in this host crystal. The Nd concentration incorporated into the crystal (1.1×10^{20} ions cm^{-3}) was determined by total-reflection x-ray fluorescence (TRXRF), with a relative error lower than 5%.

Plate samples of Nd:YAB were cut from the crystal boule with the c-axis contained either in its main faces, for σ ($E \perp c$) and π ($E \parallel c$) spectra, or perpendicular to them, for α spectra (beam $\perp c$). These faces were then carefully polished.

The polarized optical absorption spectra were measured with a Hitachi spectrophotometer (model U-3501) using a calcite polarizer.

For the fluorescence (excitation and emission) spectra a Ti-sapphire (Spectra Physics, model 3900) tunable laser was used in cw experiments, while experiments under pulsed excitation were performed by using either a high-power optical parametric oscillator (MOPO, Spectra Physics model 730) or the 337 nm line of a nitrogen laser (EG&G, model 2100). The luminescence was dispersed by a 500M SPEX monochromator (spectral resolution ~ 0.05 nm) and detected with a cooled photomultiplier or a cooled Ge detector (depending upon the spectral range). The signals were recorded by using a SR400 two-channel gated photon counter. The decay time measurements were performed using the averaging facilities of a Tektronix 2400 digital storage oscilloscope.

Low-temperature spectra (10 K) were taken by mounting the samples in a Leybold temperature controlled closed He cycle cryostat.

3. Results and discussion

As in other crystals, the absorption and luminescence spectra of Nd^{3+} in YAB consist of transitions among the Stark sublevels of $^{2S+1}L_J$ states within the $4f^3$ configuration of the ion. Figure 1 shows a simplified energy level diagram of Nd^{3+} in YAB (configured with the results reported in this work) displaying the energy gaps among the different states. The width of the lines in each state indicates the extent of the crystalline field splitting. This diagram is useful for assignment of the states involved in the different absorption/emission transitions reported in this work. Arrows indicate those states from which emissions (discussed below) have been observed in this work.

Because Nd^{3+} ions replace Y^{3+} lattice cations in yttrium aluminum borate, the incorporated Nd^{3+} ions are expected to retain the environment of the occupied lattice site, which is trigonal D_3 symmetry. Within this local symmetry all $^{2S+1}L_J$ states are split by the crystal field into the maximum number of Kramers levels $(2J + 1)/2$, which can be conveniently labelled by the crystal field quantum numbers $\mu = 1/2$ and $\mu = 3/2$.

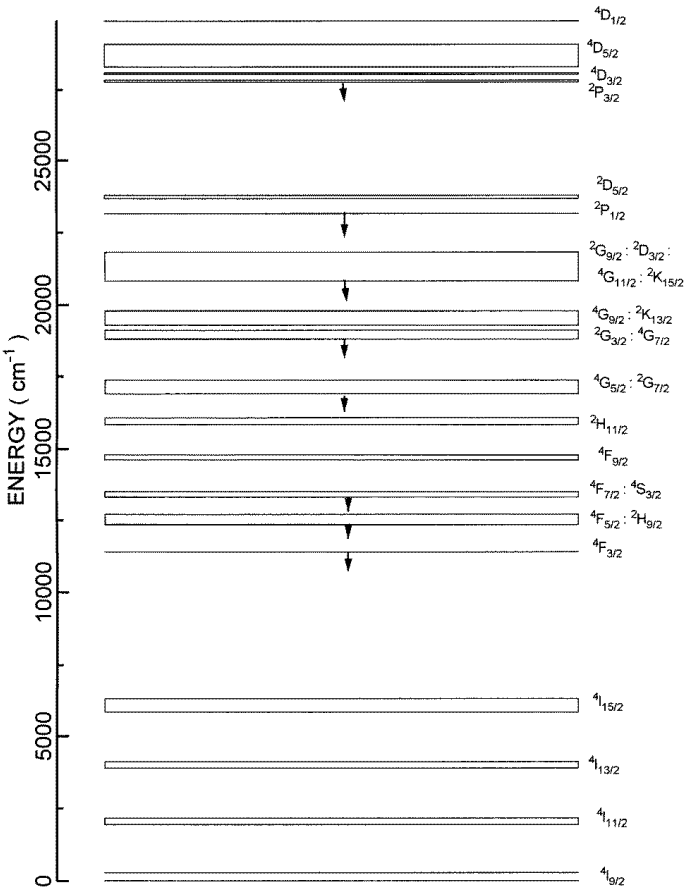

Figure 1. Energy level diagram of the Nd^{3+} ion in YAB. Arrows indicate the observed radiative emitting states.

Optical absorption and fluorescence spectra were measured both at low (LT) and at room temperature (RT).

From LT spectra the different Stark energy levels can be identified and conveniently labelled. In fact, at this temperature, thermalization effects are substantially reduced and therefore optical spectra appear greatly simplified. Most energy levels have been determined from LT absorption spectra. However, LT fluorescence spectra were also measured in order to search for additional energy levels belonging to the low-energy states which lie out of the spectral range covered by our spectrophotometer. In addition, a full analysis of the emission spectra was performed in order to identify the main radiative depopulating channels in this system.

RT absorption spectra were recorded for determination of the integrated absorption line strengths. Then, applying the Judd–Ofelt (JO) theory [17, 18] the radiative rates and branching ratios can be estimated. Once this information is obtained, laser physics parameters (stimulated emission cross section, quantum efficiency, etc) of the material can be calculated if the RT emission spectra and the fluorescence lifetimes are known.

Table 1. Energy levels, polarization character and crystal field quantum number μ of the Nd^{3+} ion in YAB. The polarization character of energy levels at 1982 and 2127 cm^{-1} has not been established with enough accuracy.

State	Energy (cm^{-1})	Character	μ
$^4I_{9/2}$	0	σ, π	1/2
	48	σ	3/2
	109	σ	3/2
	165	σ, π	1/2
	289	σ, π	1/2
$^4I_{11/2}$	1945	σ, π	1/2
	1968	σ, π	1/2
	1982	—	—
	2082	σ, π	1/2
	2127	—	—
	2165	σ, π	1/2
$^4I_{13/2}$	3900	σ, π	1/2
	3912	σ, π	1/2
	3952	σ, π	1/2
	3931	σ	3/2
	4068	σ, π	1/2
	4097	σ	3/2
	4114	σ, π	1/2
$^4I_{15/2}$	5827	σ	3/2
	5886	σ	3/2
	5973	σ, π	1/2
	6024	π	
	6130	σ, π	1/2
	6170	σ, π	1/2
	6234	σ	3/2
	6309	σ, π	1/2
$^4F_{3/2}$	11 391	σ, π	1/2
	11 440	σ	3/2
$^4F_{5/2} : {}^3H_{9/2}$	12 336	σ	3/2
	12 391	σ, π	1/2
	12 449	σ, π	1/2
	12 473	σ	3/2
	12 500	σ, π	1/2
	12 556	σ, π	1/2
	12 648	σ, π	1/2
	12 703	σ	3/2
$^4F_{7/2} : {}^4S_{3/2}$	13 313	σ	3/2
	13 370	σ, π	1/2
	13 385	σ, π	1/2
	13 428	σ, π	1/2
	13 491	σ, π	1/2
	13 500	σ	3/2
$^4F_{9/2}$	14 604	π	
	14 632	σ, π	1/2
	14 655	σ	3/2
	14 768	σ	3/2
	14 773	σ, π	1/2

Table 1. (Continued)

State	Energy (cm^{-1})	Character	μ
$^2H_{11/2}$	15 809	σ, π	1/2
	15 844	σ	3/2
	15 952	σ	3/2
	15 992	σ, π	1/2
	16 014	σ, π	1/2
$^4G_{5/2} : {}^2G_{7/2}$	16 880	σ, π	1/2
	17 050	σ, π	1/2
	17 076	σ	3/2
	17 135	σ, π	1/2
	17 188	σ, π	1/2
	17 259	σ, π	1/2
	17 352	σ	3/2
$^2G_{3/2} : {}^4G_{7/2}$	18 779	σ	3/2
	18 831	σ, π	1/2
	18 887	σ, π	1/2
	18 954	σ	3/2
	19 011	σ, π	1/2
	19 091	σ, π	1/2
$^4G_{9/2} : {}^2K_{13/2}$	19 267	σ	3/2
	19 312	σ, π	1/2
	19 387	σ	3/2
	19 398	σ, π	1/2
	19 436	σ, π	1/2
	19 469	σ	3/2
	19 488	σ, π	1/2
	19 607	σ, π	1/2
	19 723	σ, π	1/2
	19 762	σ	3/2
	19 786	σ, π	1/2
$^2G_{9/2} : {}^2D_{3/2}$	20 833	σ	3/2
$^4G_{11/2} : {}^2K_{15/2}$			
	20 048	σ	3/2
	20 947	σ	3/2
	21 225	σ, π	1/2
	21 105	σ, π	1/2
	21 133	σ	3/2
	21 195	σ	3/2
	21 235	σ	3/2
	21 326	σ	3/2
	21 413	σ, π	1/2
	21 461	σ	3/2
	21 522	σ, π	1/2
	21 598	σ, π	1/2
	21 633	σ	3/2
	21 691	σ	3/2
	21 809	σ, π	1/2
$^2P_{1/2}$	23 153	σ, π	1/2
$^2D_{5/2}$	23 666	σ, π	1/2
	23 719	σ	3/2
	23 786	σ, π	1/2

Table 1. (Continued)

State	Energy (cm^{-1})	Character	μ
$^2P_{3/2}$	27 750	σ	3/2
	27 820	σ, π	1/2
$^4D_{3/2}$	28 019	σ	3/2
	28 074	σ, π	1/2
$^4D_{5/2}$	28 270	σ, π	1/2
	28 422	σ	3/2
$^4D_{1/2}$	29 846	σ, π	1/2

3.1. Optical absorption

Detailed polarized (σ, π and α) absorption spectra of the Nd^{3+} ion in YAB crystals were recorded at low (10 K) and room temperature.

3.1.1. LT absorption spectra. Figure 2(a) shows the 10 K absorption spectrum of Nd:YAB (taken in α configuration) in the wavelength range from 300 nm to 2600 nm. The excited states involved in the different sets of transitions have been included in this figure. In addition, the polarized σ and π spectra of a plate sample containing the ferroelectric c-axis have been registered. Figure 2(b) shows, as an example, the detailed spectra related to four relevant spectral regions, where the great dependence of the spectra on the polarization of the incident light can be noticed. A careful analysis of the polarized spectra allowed us to detect most (103) energy levels of the Nd^{3+} ion in this crystal. The energy values corresponding to these levels are listed in table 1. In particular, Stark components up to 30 000 cm^{-1} of the states have been positioned. At higher energies the absorption edge becomes dominant and no more states can be accessed. The energy levels of the majority of states (all except $^4F_{3/2}$, $^4I_{13/2}$, $^4I_{11/2}$ and $^4I_{9/2}$) are detected for the first time. The energy levels corresponding to sates $^4I_{13/2}$, $^4I_{11/2}$ and $^4I_{9/2}$ are in good agreement with those previously reported [13, 15]. On the other hand, the energy levels of state $^4F_{3/2}$ (see figure 2(b)) are now resolved with great accuracy (<3 cm^{-1}), in good agreement with the emission spectra, helping to solve some discrepancies in previous literature [13, 14].

An inspection of table 1 indicates that the first excited state in $^4I_{9/2}$ is 48 cm^{-1} above the ground level. This ensures negligible population of excited levels at 10 K. Thus LT optical absorption spectra are free from transitions departing from excited levels of the ground state and the labeling of the identified energy levels is substantially simplified.

According to D_3 local symmetry around Nd^{3+} ions, the energy levels detected can be conveniently labelled by their crystal field quantum numbers, taking into account the selection rules for electric dipole (ED) transitions in the former group of symmetry. The ED character of the transitions follows from the fact that α and σ absorption spectra are quite similar. The ED selection rules in D_3 symmetry allow for σ and π character in $\mu = 1/2$ to $\mu = 1/2$ transitions, σ character in $\mu = 1/2$ to $\mu = 3/2$ transitions and π character in $\mu = 3/2$ to $\mu = 3/2$ transitions. As can be seen in figure 2(b), the σ and π polarized spectra involving the absorption transitions to the main laser state ($^4F_{3/2}$) indicate that the lowest energy level (0 cm^{-1}) is related to a crystal field quantum number $\mu = 1/2$. In fact one of the two components (11 391 cm^{-1}) shows a double (σ, π) character while the

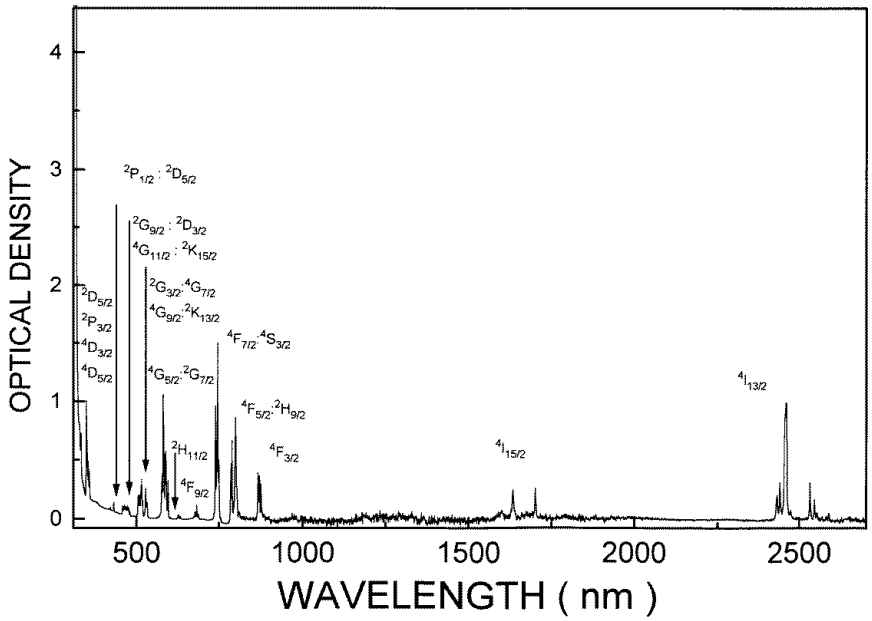

(a)

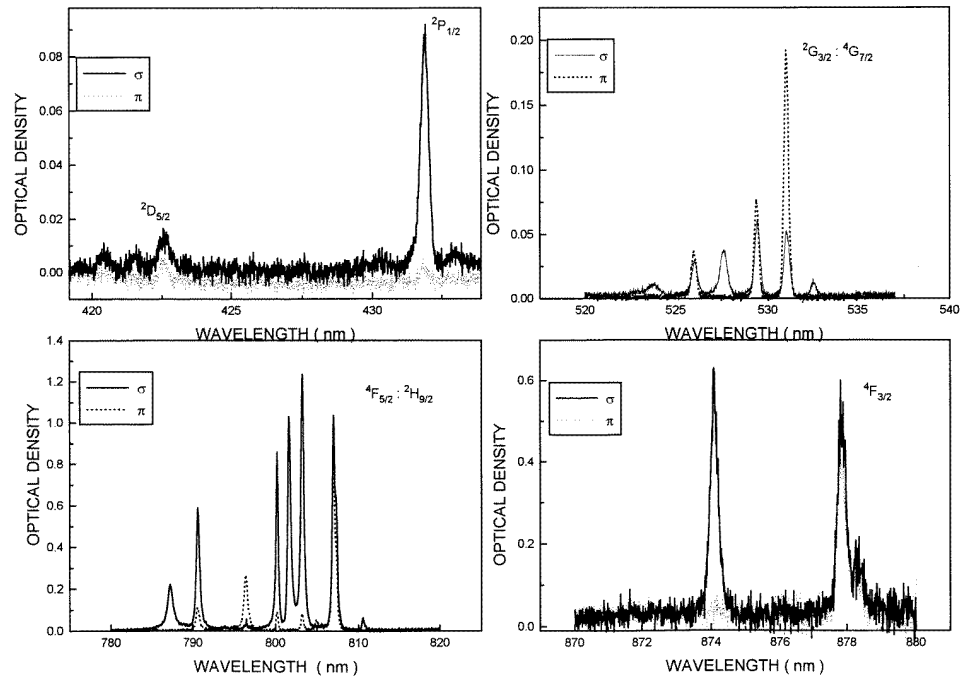

(b)

Figure 2. Low-temperature (10 K) polarized absorption spectra: (a) α configuration; (b) σ and π absorption configurations.

other one (11 440 cm^{-1}) presents a single σ character. This clearly confirms the previous assignment $\mu = 1/2$ to the ground energy level.

Consequently, the excited states can be labelled considering the D_3 local symmetry of the site occupied by Nd^{3+} ions. In table 1 the polarization characters, as well as the corresponding labelling, have been included for the energy levels identified. It can be noticed how some energy levels otherwise expected by group theory considerations do not appear. Obviously, this must be due either to coincidence (or close proximity) with other energy levels or to weakness of their associated absorption. In addition, the energy levels at 6024 cm^{-1} and 14 604 cm^{-1} show unexpected π character, which cannot be explained by local D_3 symmetry. Nevertheless, most absorption lines are in good agreement with trigonal D_3 symmetry for the Nd^{3+} active ions.

3.1.2. Room temperature absorption spectra. Judd–Ofelt intensity parameters. The polarized (σ, π and α) absorption spectra have been also carefully recorded at room temperature in order to estimate the JO intensity parameters.

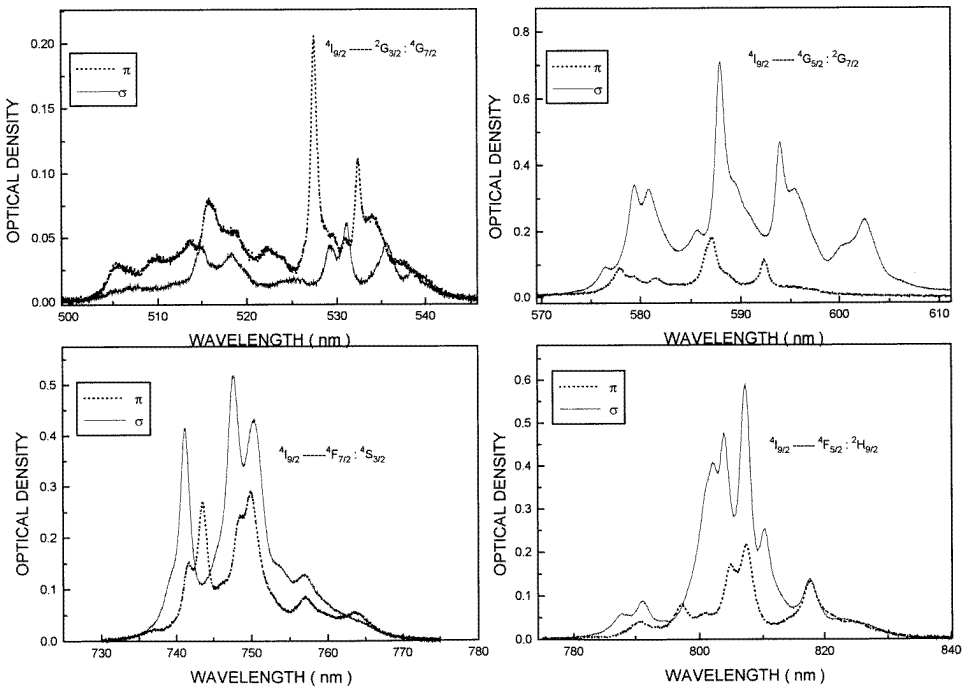

Figure 3. RT polarized (σ and π) absorption spectra.

Figure 3 shows the room-temperature σ and π absorption spectra of Nd^{3+} in YAB for the most relevant spectral regions involved in the JO analysis. In these spectra the optical lines appear less resolved than in the LT spectra (see figure 2(b)), due to thermal broadening of the absorption lines as well as appearance of hot side bands originating from population of the excited levels within the ground state $^4I_{9/2}$. This is otherwise necessary in order to be closer to the JO assumption of equal population for all the states of same J.

At this point, the absorption line strengths of ED transitions departing from the ground state $^4I_{9/2}$ can be measured, as in our case. Then the JO formalism for anisotropic crystals

[19] can be applied in order to calculate the radiative transition probabilities and branching ratios between any two states of the system.

For uniaxial crystals the absorption strength $S(J \rightarrow J')$ from the ground state ($J = 9/2$) to a particular excited state J' is given by

$$S_{ED}(J \rightarrow J') = \frac{3\cosh(2J+1)}{8\pi^3\rho\bar{\lambda}e^2}\frac{\Gamma_\pi + 2\Gamma_\sigma}{\chi_\pi + 2\chi_\sigma} \tag{1}$$

where $\rho = 1.1 \times 10^{20}$ ions cm^{-3} is the Nd^{3+} concentration in the host crystal, $\bar{\lambda}$ is the mean wavelength of the transition and $2J + 1 = 10$ is the multiplicity of the ground state. $\Gamma_{\sigma,\pi}$ are the integrated absorbances and $\chi_{\sigma,\pi} = (n^2_{\sigma,\pi} + 2)^2/9n_{\sigma,\pi}$ the Lorentz local field correction for the refractivity of the medium, where $n_\sigma = n_0$ and $n_\pi = n_e$ (taken from [4]) are assumed respectively for the ordinary and extraordinary indices at every wavelength (λ).

According to the JO theory, the line strength of any ED transition between two states J and J' can be written as

$$S_{ED}(J \rightarrow J') = \sum \Omega_t |\langle J||U^{(t)}||J'\rangle| \tag{2}$$

where Ω_t ($t = 2, 4, 6$) are the well known JO intensity parameters (that characterize the strength of the crystal field) and the matrix elements $|\langle J||U^{(t)}||J'\rangle|$ ($U^{(t)}$ being a tensor operator of rank t) are related to the free ion and can be obtained from the tables of Carnal *et al* [20]. Thus, the JO intensity parameters can be obtained by fitting the latter expression to the values of S experimentally determined by formula (1).

Making use of the absorption spectra of figure 3 the JO intensity parameters $\Omega_2 = 3.09 \times 10^{-20}$ cm^2, $\Omega_4 = 5.04 \times 10^{-20}$ cm^2 and $\Omega_6 = 3.11 \times 10^{-20}$ cm^2 were obtained by a least-squares fitting, resulting in a root mean square (rms) deviation of 0.5×10^{-20}. The parameters obtained are different from those previously reported for the same system ($\Omega_2 = 1.79\times10^{-20}$ cm^2, $\Omega_4 = 2.44\times10^{-20}$ cm^2 and $\Omega_6 = 3.25\times10^{-20}$ cm^2) [13]. However, the parameters previously reported were determined without considering the anisotropy of YAB crystal. The new set of intensity parameters obtained in this work should lead to more accurate values of laser physics parameters, like radiative transition probabilities, branching ratios quantum efficiencies and cross sections.

After the intensity parameters, Ω_2, Ω_4 and Ω_6, have been determined, the radiative transition probabilities between any pair of states can be calculated by

$$A(J \rightarrow J') = \frac{64\pi^4 e^2}{3h(2J+1)\bar{\lambda}^3}(\tfrac{2}{3}n^2_\sigma\chi_\sigma + \tfrac{1}{3}n^2_\pi\chi_\pi)S_{ED}(J \rightarrow J') \tag{3}$$

and then, the radiative lifetimes $\tau_R = (\sum A(J \rightarrow J'))^{-1}$ and branching ratios $\beta_{J\rightarrow J'} = A(J \rightarrow J')\tau_R(J)$, of great relevance to laser performance, can be estimated. Table 2 shows the ED radiative transition probabilities, branching ratios and radiative lifetimes for the laser metastable state, $^4F_{3/2}$, of Nd^{3+} in YAB. The values reported for other nonlinear SFD laser crystals have been included in this table for comparison. It should be pointed out that although the branching ratios are similar in the three systems, only the two borates, YAB and $LaBGeO_5$, display similar radiative lifetimes, which are dissimilar to that of the $LiNbO_3$:MgO crystal.

3.2. Fluorescence

3.2.1. Emission from the $^4F_{3/2}$ state. The emission spectra from the $^4F_{3/2}$ state (fluorescence and decay time) were systematically investigated in order to determine the radiative quantum efficiency and the stimulated emission cross sections for the main laser channel as well

Table 2. Spectral parameters (radiative rates, A, branching ratios, β, and radiative lifetimes, τ_r) for the $^4F_{3/2} \rightarrow {}^4I_J$ transitions of Nd^{3+} in nonlinear laser crystals for SFD, determined from the JO formalism. Experimental fluorescence lifetimes and calculated quantum efficiencies are also included.

Material	Transition	$A(J \rightarrow J')$ (s^{-1})	β	τ_r (μs)	τ (μs)	η_r
$MgO:LiNbO_3$	$^4F_{3/2} \rightarrow {}^4I_{9/2}$	4649	0.47	101.1	95	0.94
	$\rightarrow {}^4I_{11/2}$	4451	0.45			
	$\rightarrow {}^4I_{13/2}$	791	0.08			
	$\rightarrow {}^4I_{15/2}$					
$YaI_3(BO_3)_4$	$^4F_{3/2} \rightarrow {}^4I_{9/2}$	1637	0.493	302.1	53	0.18
	$\rightarrow {}^4I_{11/2}$	1430	0.431			
	$\rightarrow {}^4I_{13/2}$	235	0.071			
	$\rightarrow {}^4I_{15/2}$	12	0.005			
$LaBeGeO_5$	$^4F_{3/2} \rightarrow {}^4I_{9/2}$	1242	0.390	314.2	280	0.89
	$\rightarrow {}^4I_{11/2}$	1604	0.505			
	$\rightarrow {}^4I_{13/2}$	320	0.100			
	$\rightarrow {}^4I_{15/2}$	16	0.005			

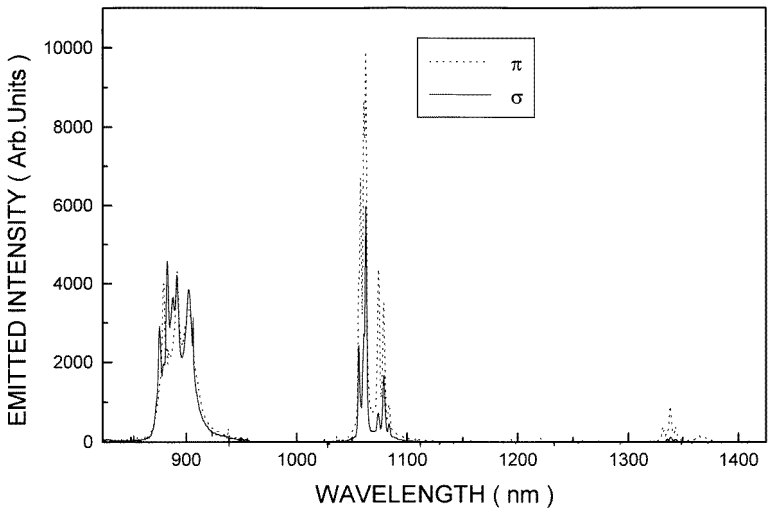

Figure 4. RT polarized emission spectra in the infrared spectral domain obtained under excitation at 750 nm.

as for detecting those additional energy levels which were not accessible by absorption spectroscopy.

Figure 4 shows the RT polarized emission spectra from state $^4F_{3/2}$ to the terminal states $^4I_{9/2}$, $^4I_{11/2}$ and $^4I_{13/2}$ (the emission to state $^4I_{15/2}$ was not accessible to our detectors). These emission spectra were also taken at 10 K in order to determine the energy levels of these terminal states. The positions of the energy levels determined from these emission spectra are included in table 1. In fact these energy levels were not directly accessible from the absorption spectra. Moreover it must be noted from the table that the character of some energy levels of state $^4I_{11/2}$ is not well established. This is due to the lesser accuracy in

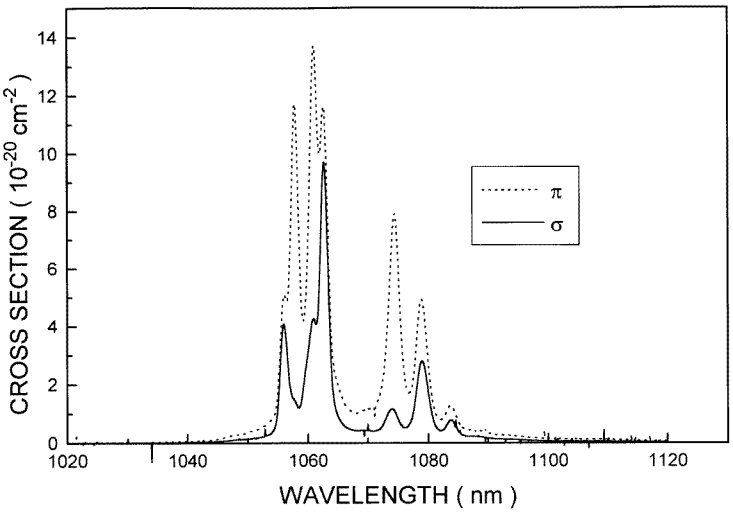

Figure 5. Spectral dependence (RT) of the stimulated emission cross section calculated from the $^4F_{3/2} \rightarrow {}^4I_{11/2}$ emission spectrum.

determining polarization degrees from fluorescence measurements.

The radiative quantum efficiency from the metastable state $^4F_{3/2}$ can be determined if the fluorescence lifetime is known. Our crystals showed an exponential decay with a lifetime of 56 (± 2) μs, which is basically temperature independent in the range from 15 to 300 K. Comparing this value with the radiative lifetime predicted by the JO analysis, a quantum efficiency of about 18% is obtained. This value is greater than that previously reported by using an isotropic JO theory (14%) [13]. In any case the radiative quantum efficiency is lower (see table 2) than in the other nonlinear crystals of interest for SFD. It has been previously proposed [13] that this low quantum efficiency can be related to the high energy of the effective phonons (1346 cm^{-1}). Multiphonon decay from the state $^4F_{3/2}$ to the next lower state $^4I_{15/2}$ is more likely in this system than in the others shown in table 2.

Focusing on the main laser channel $^4F_{3/2} \rightarrow {}^4I_{11/2}$, once the branching ratios β and radiative lifetime τ_r are known, the spectral dependence of the stimulated emission cross section can be determined from the polarized fluorescence spectra (see figure 4), according to the expression [21, 22]

$$\sigma_e^p(\lambda) = \frac{3\lambda^5 \beta_J I^p(\lambda)}{8\pi n_p^2 c \tau_r \int \lambda (2I^\sigma(\lambda) + I^\pi(\lambda)\, d\lambda} \tag{4}$$

where λ is the emission wavelength, $I_p(\lambda)$ ($p = \sigma$ or π) the emission intensity as a function of wavelength, c the speed of light and n_p ($p = \sigma$ or π) the material refractive indices. Figure 5 shows the spectral dependence (σ and π) of the stimulated emission cross section obtained from polarized emission spectra. The calculated peak cross sections are $\sigma_\pi = 1.4 \times 10^{-19}$ cm^2 (at $\lambda = 1061$ nm) and $\sigma_\sigma = 1 \times 10^{-19}$ cm^2 (at $\lambda = 1062.6$ nm), which are of the order of those reported for $LiNbO_3$:Mg:Nd [23] and $LaBGeO_5$:Nd [10, 12].

3.2.2. Visible luminescence. In order to identify the rest of the emission channels different from the main infrared ones, the emission spectra were systematically investigated under laser excitation at different wavelengths. As an example, figure 6 shows the visible RT

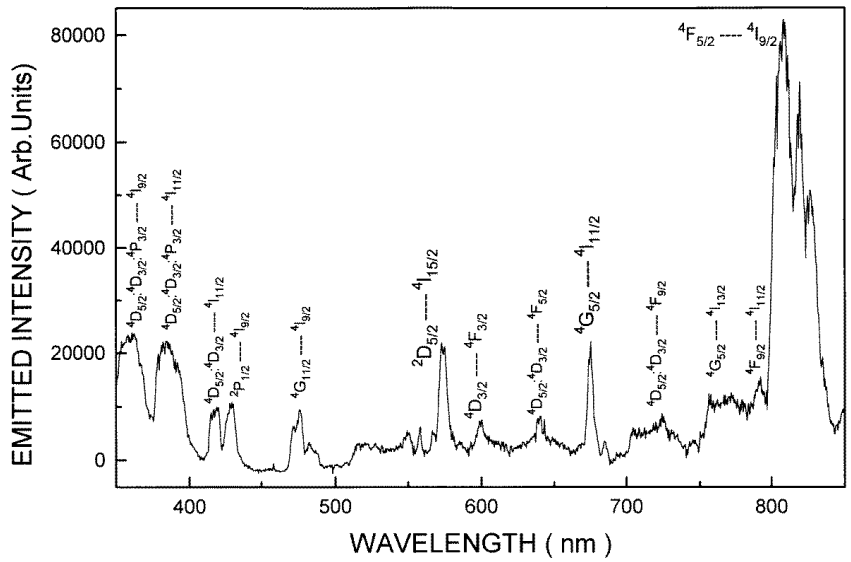

Figure 6. RT unpolarized emission spectrum in the visible domain under excitation at 337 nm.

emission spectrum obtained under excitation at 337 nm. A great number of visible lines are observed, corresponding to transitions from different excited states. The identified depopulating channels appear displayed also in this figure. Laser excitation at other wavelengths produces emissions from several excited states. The emitting states identified in this work have been indicated on the energy level diagram of figure 1.

3.2.3. Up-converted luminescence. Excited state absorption (ESA) of pump or laser radiation can lead to considerable losses in the laser gain. Further, ESA can result in multiphonon relaxation processes increasing the temperature of the laser crystal. Information on the relevance of ESA of pump radiation can be partially obtained by investigating the infrared (IR) to visible up-converted luminescence, which is typically observed in Nd-doped systems. In fact, this visible up-converted luminescence is often used to focus the pump beam in end-pumped lasers.

We have performed systematic research of the IR to visible up-converted luminescence in the spectral region of interest for diode pumping (720 to 820 nm).

Figure 7(a) shows the RT emission spectrum obtained under excitation at 810 nm. The up-converted visible emission spectrum consists of three structured bands centred around 535 nm, 590 nm and 675 nm. These emission bands can be assigned to transitions from several excited states that appear to be populated by processes that involve more than one pump photon. The dependence of the visible emission bands on the excitation intensity displays a near-quadratic (slope 2.05) dependence, which is in good agreement with the higher-order process of the excitation mechanism.

The emission centred at 535 nm can be tentatively assigned to spin-allowed transitions from the $^4G_{7/2}$ state to the ground state $^4I_{9/2}$. In fact, the former metastable excited state explains also the emission band centred at 590 nm via $^4G_{7/2} \rightarrow {}^4I_{11/2}$ transitions. However, in both cases, some contributions arising from the $^4G_{11/2}$ state (and those that are mixed with it and have spin multiplicity 2, see the diagram in figure 1) cannot be completely

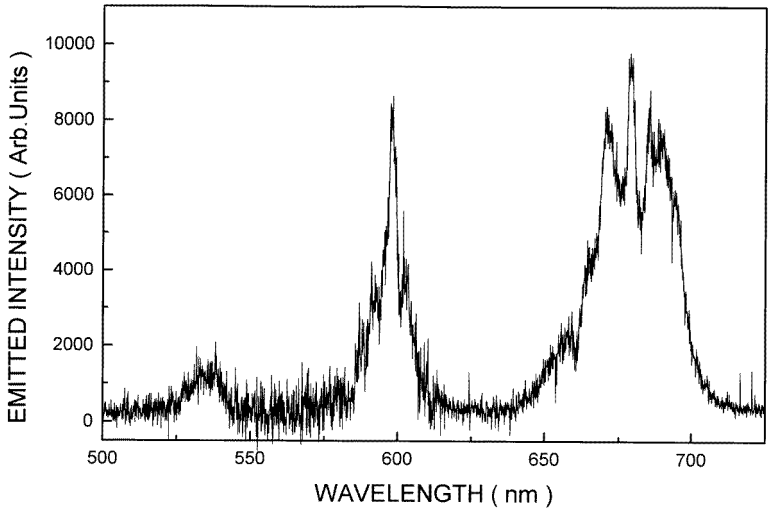

(a)

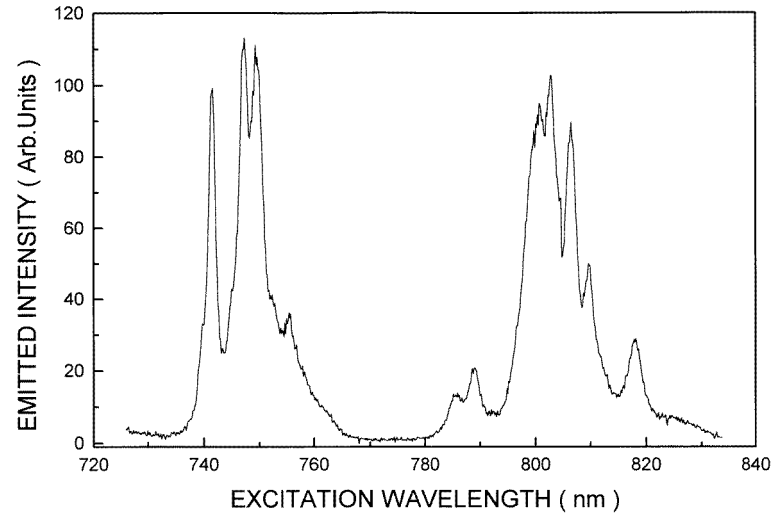

(b)

Figure 7. (a) RT up-converted emission spectrum obtained under excitation at 810 nm. (b) RT excitation spectrum of the visible up-converted luminescence (emission wavelength at 590 nm).

disregarded. Finally the emission centred at 675 nm may involve a variety of transitions departing from several excited states (mainly the states $^4G_{7/2}$, $^4G_{5/2}$ and $^4F_{9/2}$) to the states $^4I_{11/2}$ and $^4I_{9/2}$. The shape shown of this band is distorted by the use of an infrared filter to avoid overlapping with the much more intense infrared transitions departing from the metastable state $^4F_{3/2}$.

In spite of the fact that a final identification of the transitions involved in the up-converted visible emission spectrum cannot be given, the contribution of several depopulating channels mainly departing from the excited states $^4G_{7/2}$, $^4G_{5/2}$ and $^4F_{9/2}$ is

clear. This behaviour is reasonably expected by taking into account the energy gap law [24] and the quartet spin multiplicity of these states.

Let us now discuss the possible mechanism to populate the excited states (mainly the $^4G_{7/2}$) from which the up-converted emission spectrum originates. In principle two mechanisms could be responsible for the population of these states [25]: ESA of two pump photons or an energy transfer up-conversion process.

Figure 7(b) shows the excitation spectrum observed for the 590 nm up-converted luminescence in the wavelength spectral range for diode-pumping. This spectrum displays a quite similar shape to the absorption spectrum (as given by absorbance against wavelength). This fact seems to indicate that there is no modulation of the first photon absorption spectrum by the second photon absorption spectrum. In fact, the up-converted excitation spectrum of figure 7(b) cannot be explained with the sequential absorption of two pump photons since no electronic states of ion Nd^{3+} in YAB are available (as can be tested by figure 1 or table 1). For instance, excitation at 750 nm (to the states $^4F_{7/2}$ and $^4S_{3/2}$) does not match any excited state of Nd^{3+} by absorption of a second photon of 750 nm, neither from states $^4F_{7/2}$: $^4S_{3/2}$ nor from the metastable state $^4F_{3/2}$, which is reached after the expected non-radiative relaxation (see figure 1). Therefore this fact indicates that ESA of pump photons from the metastable state $^4F_{3/2}$ is negligible. Thus, an energy transfer up-conversion process seems to be more reasonable to account for the population of the excited states responsible for the visible up-converted luminescence. In this process two nearby excited Nd^{3+} ions in the $^4F_{3/2}$ state undergo an energy transfer process, leaving one ion in one of the terminal states $^4I_{13/2}$ or, more likely, $^4I_{11/2}$. This mechanism is also in agreement with the relatively high Nd concentration of our crystals. Another possibility that cannot be completely discarded to populate the up-conversion excited states is a radiation transfer up-conversion, in which a fluorescence photon is absorbed by another Nd^{3+} ion in the excited state $^4F_{3/2}$.

Additional experiments are under way in our laboratory, in order to have a full understanding of the mechanism responsible for the observed up-conversion fluorescence.

Acknowledgments

This paper has been supported by the Comisión Interministerial de Ciencia y Tecnología (CICYT) under project MAT 95/152. D Jaque holds a grant from Ministerio de Educación y Ciencia.

References

[1] Lin J T 1990 *Laser Optron.* December 35
[2] Lin J T 1990 *Opt. Quant. Electron.* **22** S283
[3] Luo Zundu, Jiang Aidong, Huang Yichan and Qiu Minwang 1989 *Chin. Phys. Lett.* **6** 440
[4] Lu Bao-sheng, Wang Ju, Pan Heng-fu, Jiang Min-hua, Liu En-quan and Hou Xue-yuan 1989 *J. Appl. Phys.* **66** 6052
[5] Tingjie Z, Zundu L, Yichuan H, Min Wang Q and Guang C 1994 *Opt. Commun.* **109** 115
[6] Hemmati H 1992 *IEEE J. Quantum Electron.* **QE-28** 1169
[7] Li Zhenhua, Fan Qikang, Zhou Fuzheng, Ma Jianwei and Xue Qiang 1994 *Opt. Eng.* **33** 1138
[8] Fan T Y, Cordova-Plaza A, Digonnet M J F, Nyer R L and Shaw H J 1986 *J. Opt. Soc. Am.* B **3** 140
[9] Capmany J, Bausá L E, Jaque D, García Solé J and Kaminskii A A 1997 *J. Lumin.* **72–74** 816
[10] Moncorgé R, Guyot Y, Boulon G, García Solé J, Capmany J, Kaminskii A A, Butashin A V and Mill B V 1994 *J. Physique Coll.* IV C **4** 423
[11] Capmany J, Bausá L E, García Solé J, Moncorgé R, Butashin A V, Mill B V and Kaminskii A A 1994 *J. Lumin.* **60/61** 78

[12] Capmany J 1996 *Doctoral Thesis* Universidad Autónoma de Madrid
[13] Pan Heng-fu, Liu Ming-guo, Xue Jing and Lu Bao-sheng 1990 *J. Phys.: Condens. Matter* **2** 4525
[14] Huang Yidong and Luo Zundu 1991 *Phys. Status Solidi* b **167** K117
[15] Luo Zundu and Huang Yidong 1993 *J. Phys.: Condens. Matter* **5** 6949
[16] Luo Z D, Lin J T, Hang A D, Huang Y C and Qui M W 1989 *Proc. SPIE* **1104** 132
[17] Judd B R 1962 *Phys. Rev.* **127** 750
[18] Ofelt G S 1962 *J. Chem. Phys.* **37** 511
[19] Lomheim T S and DeShazer L G 1978 *J. Appl. Phys.* **49** 5517
[20] Carnal W T, Fields P R and Rajnak K 1968 *J. Chem. Phys.* **49** 4422
[21] Singh S, Smith R G and Van Uitert L G 1974 *Phys. Rev.* B **10** 2566
[22] Aull B F and Jenssen H P 1982 *IEEE J. Quantum Electron.* **QE-18** 925
[23] Burlot R, Moncorgé R, Manaa H, Boulon G, Guyot Y, García Solé J and Cochet-Muchy D 1996 *Opt. Mater.* **6** 313
[24] Henderson B and Imbusch G F 1989 *Optical Spectroscopy of Inorganic Solids* (Oxford: Clarendon)
[25] Chuang Ti and Verdún H R 1996 *IEEE J. Quantum Electron.* **32** 79